Cancer Chemotherapy and Pharmacology (2019) 83:151–160
https://doi.org/10.1007/s00280-018-3716-3

ORIGINAL ARTICLE

Nonclinical pharmacokinetics and in vitro metabolism of H3B-6545, a novel selective ERα covalent antagonist (SERCA)

Nathalie Rioux[1,2] · Sherri Smith[1] · Manav Korpal[1] · Morgan O'Shea[1] · Sudeep Prajapati[1] · Guo Zhu Zheng[1] · Markus Warmuth[1] · Peter G. Smith[1]

Received: 26 September 2018 / Accepted: 25 October 2018 / Published online: 1 November 2018

Abstract

Purpose H3B-6545, a novel selective estrogen receptor (ER)α covalent antagonist (SERCA) which inactivates both wild-type and mutant ERα, is in clinical development for the treatment of metastatic breast cancer. Preclinical studies were conducted to characterize the pharmacokinetics and metabolism of H3B-6545 in rat and monkeys.

Methods The clearance and metabolic profiles of H3B-6545 were studied using rat, monkey and human hepatocytes, and reaction phenotyping was done using recombinant human cytochrome P450 enzymes. Blood stability, protein binding, and permeability were also determined in vitro. Pharmacokinetics of H3B-6545 was assessed after both intravenous and oral dosing. A nonclinical PBPK model was developed to assess in vitro–in vivo correlation of clearance.

Results H3B-6545 had a terminal elimination half-life of 2.4 h in rats and 4.0 h in monkeys and showed low to moderate bioavailability, in line with the in vitro permeability assessment. Plasma protein binding was similar across species, at 99.5–99.8%. Nine metabolites of H3B-6545 were identified in hepatocyte incubations, none of which were unique to humans. Formation of glutathione-related conjugate of H3B-6545 was minimal in vitro. H3B-6545, a CYP3A substrate, is expected to be mostly cleared via hepatic phase 1 metabolism. Hepatocyte clearance values were used to adequately model the time-concentration profiles in rat and monkey.

Conclusions We report on the absorption and metabolic fate and disposition of H3B-6545 in rats and dogs and illustrate that in vitro–in vivo correlation of clearance is possible for targeted covalent inhibitors, provided reactivity is not a predominant mechanism of clearance.

Keywords H3B-6545 · Pharmacokinetics · Metabolism · Breast cancer · Covalent antagonist

Introduction

Breast cancer is the second leading cause of cancer mortality among women worldwide with more than 1 million new cases diagnosed each year and approximately 400,000 deaths annually [1]. Approximately 70% of breast cancers express estrogen receptor alpha (ERα), a key hormone-regulated transcription factor for normal and malignant breast cells. Nonclinical and clinical epidemiological studies highlight an important oncogenic role for ERα in the genesis and progression of breast cancer [2]. Several ER-directed therapies have been developed to antagonize oncogenic ERα function including selective ER modulators or down-regulators, selective nonsteroidal aromatase inhibitors, and steroidal aromatase inhibitors [3], for use in women with locally advanced, recurrent or metastatic cancer. Although these therapies have demonstrated anti-tumor efficacy in the clinic, innate and acquired resistance remains a major challenge. The recurrent mutations in ERα, which are enriched in nearly 30% of endocrine-therapy resistant metastases, are associated with shorter overall survival relative to the wild-type ESR1 [4], and confer partial resistance to endocrine therapies. Using a structure-based drug design approach, H3B-5942 was recently identified as a representative compound from a novel class of ERα antagonists referred to as selective ERα covalent antagonist (SERCA), which inactivates both wild-type and mutant ERα [5].

✉ Nathalie Rioux
Nathalie_rioux@h3biomedicine.com;
nathalie.rioux@certara.com

[1] H3 Biomedicine Inc, 300 Technology Square, Cambridge, MA 02139, USA

[2] Certara Strategic Consulting, Cambridge, MA, USA

Targeted covalent inhibitors (TCI), such as H3B-5942, are attractive for potential enhanced biochemical efficacy, duration of action, and selectivity, all attributes associated with their irreversible inhibition mechanism. From a DMPK perspective, nonclinical in vitro–in vivo correlation (IVIVC) for the prediction of clearance (CL), and subsequently human pharmacokinetic (PK) projection, may be challenging for TCIs due to their potential for glutathione (GSH) conjugation, and potential nonspecific binding. These occur by non-enzymatic and/or GSH-*S*-transferase (GST)-mediated mechanisms, in both the liver and extrahepatic tissues [6]. Consequently, data extrapolated from traditional matrices employed in in vitro CL assays such as liver microsomes, S9 fractions, or hepatocyte incubations are typically not representative of in vivo CL. We recently reported that good IVIVC is achievable for TCIs with minimal extrahepatic CL such as H3B-5942, a representative SERCA [7]. Following medicinal chemistry optimization in this indazole series, H3B-6545 was discovered [8]. In vivo, H3B-6545 demonstrated significant single agent anti-tumor activity in xenograft mouse models representing $ER\alpha^{WT}$ and $ER\alpha^{Y537S}$ breast cancer [8]. H3B-6545 is currently undergoing evaluation in a global multicenter Phase I/II clinical trial in women with locally advanced or metastatic estrogen receptor-positive, HER2 negative breast cancer (ClinicalTrials.gov Identifier: NCT03250676).

This report describes the nonclinical PK and metabolism of H3B-6545, a novel SERCA. In vitro and in vivo studies were performed to characterize the oral bioavailability and route of metabolism of H3B-6545 in rat, dog and/or human. A nonclinical PBPK model was developed to assess in vitro–in vivo correlation of clearance. This work was key for selection of nonclinical safety species, towards projection of human PK and selection of dosing regimen in the ongoing Phase I/II clinical trial.

Methods

Chemicals

H3B-6545 ((2*E*)-*N,N*-dimethyl-4-{[2-({5-[(1*Z*)-4,4,4-trifluoro-1-(3-fluoro-1*H*-indazol-5-yl)-2-phenylbut-1-en-1-yl]pyridin-2-yl}oxy)ethyl]amino}but-2-enamide) hydrochloride salt (the clinical form) and H3B-108945, an authentic metabolite standard of H3B-6545, were synthesized by H3 Biomedicine Inc. (Cambridge, MA). All other reagents were purchased from sources as described below. Chemicals were reagent grade or better.

Metabolism by substrate depletion in rat, monkey and human hepatocytes

Pooled, female cryopreserved Sprague–Dawley rat, cynomolgus monkey and human hepatocytes (BioIVT, Baltimore, MD) were thawed in a water bath set to maintain a temperature of 37 °C. Hepatocytes were suspended at 1×10^6 viable cells/mL in hepatocyte maintenance media. H3B-6545 was added to the cells at 0.3 and 1.0 µM (< 1% organic solvent), and duplicate incubations were performed in a humidified atmosphere with 5% CO_2 at 37 °C, with agitation. Samples were taken at 0, 15, 30, 60, 120 and 180 min, quenched with acetonitrile containing a structural analog as internal standard (IS), and centrifuged for 10 min at 4000 rpm. Metabolic competency of the hepatocytes was assessed in parallel using diclofenac and metoprolol. Samples were analyzed by liquid chromatography with mass spectrometry (LC–MS/MS) using a multiple reaction monitoring (MRM) method. Depletion rate constants (k_{dep}; min-1) and squared correlation coefficients (r^2) were determined by linear regression (GraphPad Prism 6) of time (min) vs. the natural log (ln)% of H3B-6545 remaining. The k_{dep} value was used for intrinsic clearance (CL_{int}) calculation using species-dependent scaling factors [9, 10], while scaled hepatic CL were calculated as $CL_H = (Q_H \times CL_{int})/(Q_H + CL_{int})$. Extraction ratios is the ratio of CL_H/Q_H, where Q_H is the species hepatic blood flow. Unbound CL_H or $CL_{H,unbound}$ was estimated using the following equation: $CL_{H,unbound} = (Q_H \times CL_{int} \times f_u)/(Q_H + CL_{int} \times f_u)$, where f_u is the unbound fraction in plasma proteins.

In vitro metabolism of H3B-6545 in rat, monkey and human hepatocytes

H3B-6545 (10 µM, 0.2% final organic content) was incubated with pooled female Sprague–Dawley rat, cynomolgus monkey, and human hepatocytes (BioIVT, 500,000 cells per incubation) for 0, 60, and 240 min in a humidified atmosphere with 5% CO_2 at 37 °C. At each time point, the samples were quenched with an equal volume of acetonitrile and centrifuged at 4000 rpm for 10 min. A control sample was prepared by adding the compound in hepatocyte maintenance media only (without cells). Verapamil (2 µM) was used as a positive control in each species. The system for metabolite profiling and identification consisted of a Waters Acquity UPLC and a Waters Synapt G2-S high resolution MS. Samples were analyzed on a Waters Acquity BEH C18, 2.1 × 100 mm, 1.7 µm particle size, set a 60 °C. Metabolites were separated with a gradient of 10 mM ammonium bicarbonate (phase A)

versus acetonitrile (phase B) at a flow rate of 500 µL/min (gradient of 95% A for 0.5 min, linear to 40%A at 8 min, linear to 5% A at 9 min with plateau to 10.25 min). H3B-6545 major fragmentation pathways were proposed and the elemental compositions of the corresponding fragment ions were confirmed. MS chromatograms operated in a full scan positive ionization mode with an acquired range of 100–1000 Da. MS full scan data were processed by Metabolynx™ to identify metabolites. Manual data mining was also used to search for unique biotransformations. Product ion spectra were then acquired, by a separate analysis, for the molecular ions of the potential metabolites. Following this initial metabolite identification study, H3B-108945, a reference standard for the *N*-desmethyl metabolite of H3B-6545, was synthesized at H3 Biomedicine. Its presence was confirmed in rat plasma samples (unpublished data on file, H3 Biomedicine) based on matching retention time and characteristic mass spectral fragment ions common between H3B-6545 and H3B-108945.

Identification of human cytochrome P450 enzymes metabolizing H3B-6545 with prediction of contributions to hepatic CYP-mediated clearance

H3B-6545 (30 nM and 100 nM) was incubated at 37 °C for 0, 1, 3, 15, 30, 60, and 120 min with human liver microsomes (HLM) and a panel of 10 recombinant human cytochrome P450 (CYP) enzymes: CYP1A2, CYP2B6, CYP2C8, CYP2C9, CYP2C19, CYP2D6, CYP2E1, CYP2J2, CYP3A4, and CYP3A5, at 0.25 mg/mL protein (Supersomes™, Corning, Woburn, MA), in 100 mM sodium phosphate buffer (pH 7.4) supplemented with 1 mM NADPH. A positive control, carvedilol (30 nM), was similarly incubated with these matrices. Incubations with control (no CYP) membrane were also performed. The reaction samples were analyzed by LC-MS/MS using a structural analog of H3B-6545 as IS. First-order depletion rate constants of H3B-6545 were determined and used to calculate CL_{int}. The relative activity factor approach [11] was then used to predict the fraction metabolized (f_m) by a particular CYP to the total hepatic CYP-mediated clearance of H3B-6545.

In vitro evaluation of the substrate potential of H3B-6545 for P-glycoprotein and breast cancer resistance protein

Evaluation of H3B-6545 (0.3, 3, and 20 µM) as a substrate of P-glycoprotein (P-gp) and breast cancer resistance protein (BCRP) was conducted in multi-drug resistance protein 1-Madin Darby Canine Kidney (MDR1-MDCK) (US National Institutes of Health, Bethesda, MD), BCRP-MDCK (Absorption Systems, Exton, PA) and control MDCK (non-transfected) cells. To reduce non-specific binding, the containers used for preparing H3B-6545 dosing solutions were rinsed with the incubation media Hank's balanced salt solution pH 7.4 supplemented with 1% weight/volume bovine serum albumin containing H3B-6545 at the corresponding concentration. Costar Transwell® plates (Corning, Oneonta, NY) were used to grow cell monolayers for the permeability studies. Potential effects of 10 and 20 µM H3B-6545 on cell monolayer integrity were assessed by co-incubation with 200 µM lucifer yellow for 150 min. Bidirectional permeability, apical-to-basolateral (AP-to-BL) and basolateral-to-apical (BL-to-AP) were assessed over time to characterize both permeability rate as well as efflux potential. For the transport assay, aliquots of fresh dosing solution (0.55 mL for AP-to-BL, 1.55 mL for BL-to-AP) were added to the donor compartment, and HBSS buffer (1.5 mL for AP-to-BL, 0.5 mL for BL-to-AP) were added to the receiver compartment. Aliquots of donor (50 µL) and receiver samples (300 µL) were taken at 0, 60 and 120 min. The apparent permeability coefficient (P_{app}) was calculated and the efflux ratios [$P_{app(BL-to-AP)}$ over $P_{app(AP-to-BL)}$] were determined. As controls, the transport of digoxin (10 µM, a P-gp substrate) and cladribine (10 µM, a BCRP substrate) was also measured in the absence or presence of valspodar (1 µM, a P-gp inhibitor) or Ko143 (0.5 µM, a BCRP inhibitor), respectively [12, 13]. The concentrations of H3B-6545 and probe substrate were determined by LC–MS/MS.

Determination of binding of H3B-6545 to rat, monkey and human plasma proteins

An ultracentrifugation approach, where unbound compound is separated from protein-bound compound by sedimentation of the proteins, was used to determine the binding of H3B-6545 to plasma proteins. Pooled blank plasma aliquots (K_2EDTA) from female SD rats, cynomolgus monkeys, and humans (BioIVT, Westbury, NY) were spiked with H3B-6545 to achieve nominal concentrations of 1, 3, and 10 µM. The pH of all matrices was adjusted to 7.4 prior to addition of H3B-6545. A control was included to assess compound recovery (stability) under the assay conditions. Compound-spiked matrix was incubated at 37 °C for 10 min and duplicate samples were transferred into polycarbonate ultracentrifuge tubes, placed into a pre-warmed Beckman TLA-100.4 rotor and centrifuged at 500,000×*g* for 2.5 h at 37 °C. Following the ultracentrifugation, any lipid layer was removed and 50 µL aliquots of supernatant were transferred to a microtiter plate containing an equal volume of blank plasma matrix for matrix-matching purposes. Reactions were stopped by addition of 300 µL of acetonitrile containing an IS. Samples were analyzed by LC–MS/MS. Calculations were performed using peak area ratios. Warfarin was used as positive control.

Determination of binding of H3B-6545 to human liver microsomes

An equilibrium dialysis method was used to measure the extent of H3B-6545 binding to HLM. H3B-6545 (1 μM) was spiked in triplicate into 0.5, 1.0, and 2.0 mg/mL of HLM in buffer and added to one side of the dialysis membrane, while buffer containing no drug was added to the other side. Incubations were carried out in a humidified atmosphere with 5% CO_2 at 37 °C while shaking for 4.5 h, prior to removing HLMs and buffer aliquots from each side of the dialysis membrane. To compensate for potential differences in ionization response signal, equal volumes of blank matrix were added to each aliquot to generate matrix-matched samples. Reactions were stopped by addition of organic solvent containing an IS. Samples were analyzed by LC–MS/MS. Calculations were performed using peak area ratios against a standard curve. Verapamil was used as positive control.

Pharmacokinetics

All animal studies were performed in accordance with the AAALAC International and NIH guidelines standards.

Female Sprague–Dawley rats (jugular-vein cannulated, 229–242 g, Envigo RMS South Easton, MA; $n = 4$ per group) were dosed with H3B-6545 intravenously (IV, Group 1) at 5 mg/kg and orally (PO, Group 2) at 10 mg/kg, after fasting overnight and through 4 h postdose. Animals were weighed prior to dose administration. IV formulation consisted of H3B-6545 in 10% (w/v) hydroxypropyl-ß-cyclodextrin in 5% (w/v) dextrose in water, whereas H3B-6545 was formulated in 0.5% (w/v) methylcellulose with 0.1% (v/v) Tween® 80 in water for PO dosing. In both cases, the target dose volume was 5 mL/kg. Serial blood samples were collected via the jugular-vein cannula, prior to dosing and at 0.0833 (Group 1 only), 0.25, 0.5, 1, 2, 4, 8 and 24 h after dosing. Blood samples were collected into K_2EDTA tubes and placed on wet ice until centrifuged (approximately 3500 rpm at 5 °C) within 1 h of collection. Plasma and dose formulation samples, stored at below − 70 °C, were analyzed for H3B-6545 using a qualified LC–MS/MS method, with a lower limit of quantitation (LLOQ) of 0.5 ng/mL. For Group 1 rats only, housed in metabolic cages, urine was collected from each animal into pre-weighed labeled containers, which were surrounded by cold packs, from 0 to 4, 4 to 8, and 8 to 24 h after dosing. Samples were stored in at below − 70 °C freezer until analysis by LC–MS/MS.

Non-naïve female cynomolgus monkeys (3.10–4.20 g; MPI Research stock colony, Mattawan, MI; $n = 4$ per group) were dosed with H3B-6545 intravenously (IV, Group 1) at 5 mg/kg and orally (PO, Group 2) at 10 mg/kg after overnight fasting prior to dosing and through 4 h postdose. H3B-6545 was formulated as described above. Animals were weighed prior to dose administration. Blood samples (approximately 1 mL) were collected via the femoral vein/artery predose, and at 0.067 (IV only), 0.167 (IV only), 0.5, 0.75, 1, 2, 4, 6, 8, 12, and 24 h postdose, in tubes maintained on ice and containing K_2EDTA as an anticoagulant. Blood was centrifuged (4 °C) and resulting plasma was stored at below − 70 °C prior to being analyzed for H3B-6545 using a qualified LC–MS/MS method (LLOQ 1.0 ng/mL).

PK parameters were determined using individual plasma concentration versus time profiles using Phoenix WinNonlin (Certara, Princeton, NJ). Standard non-compartmental PK methods were used to calculate the area under the plasma concentration–time curve (AUC) using the linear trapezoidal method. The acceptance criteria for terminal half-life determination include regression of at least three time points in the elimination phase and $r^2 > 0.9$. Nominal sample times were used in the PK analysis. Parent excretion in urine was calculated as the % dose excreted = sum of (urine concentration × urine volume), divided by dose.

Projection of human clearance and volume of distribution

A physiologically based PK (PBPK) modeling approach was used to simulate H3B-6545 exposures in rat and monkey following a single IV administration and project human CL and V_{ss}. H3B-6545 PK, plasma protein binding, hepatocytes CL data (Tables 1, 2), as well as, in silico and in vitro physicochemical properties were used to simulate exposures by PBPK modeling using GastroPlus™, version 9.0 (Simulation Plus, Inc). Measured logD (3.2) and pKa (7.4) values were input for the model. Partition coefficients were set using the Lucakova (Rodgers–Single) equation for perfusion limited tissues (option base 2). Total clearance consisted of hepatic, scaled from hepatocyte incubations at 1 μM, and renal clearance. Hepatic clearances were modeled while applying correction for plasma protein binding and an estimation of the free fraction in the in vitro hepatocyte assay. Renal clearance was set as passive renal filtration, i.e. free fraction × glomerular filtration rate, which was in line with the value measured in the rat PK. Mean human parameters were simulated based on a 35 year old Caucasian female (77 kg body weight) PK model.

Results

In vitro clearance by substrate depletion in rat, monkey and human hepatocytes

Moderate to high depletion of H3B-6545, at concentrations of 0.3 μM and 1.0 μM were observed in rat, monkey, and human hepatocyte incubations (Table 1). A modest decrease

Table 1 Cross-species in vitro clearance in hepatocytes and plasma protein binding

	H3B-6545 (μM)	Rat	Monkey	Human
$CL_{H,int}$ hepatocytes (mL/min/kg)	0.3	92	242	76
Scaled hepatic CL_H (mL/min/kg) [a]		40	37	16
Extraction ratio CL_H/Q_H (%)		57	85	79
Scaled $CL_{H,unbound}$ (mL/min/kg)		0.18	1.2–1.4	0.15–0.23
$CL_{H,int}$ hepatocytes (mL/min/kg)	1.0	72	178	74
Scaled hepatic CL_H (mL/min/kg)		36	29	16
Extraction ratio CL_H/Q_H (%)[a]		51	66	78
Scaled $CL_{H,unbound}$ (mL/min/kg)		0.14	0.42–0.50	0.15–0.22
Plasma protein binding (% bound)	1–10	99.8	99.5–99.6	99.7–99.8

CL_H hepatic clearance, f_u fraction unbound in plasma, Q_H hepatic blood flow

[a]$CL_H = (Q_H \times CL_{int})/(Q_H + CL_{int})$, $CL_{H,unbound} = (Q_H \times CL_{int} \times f_u)/(Q_H + CL_{int} \times f_u)$

Table 2 Nonclinical plasma pharmacokinetic parameters for H3B-6545 in female rats and cynomolgus monkey following intravenous and oral gavage administration

Parameter (units)	Sprague–Dawley rats		Cynomolgus monkeys	
	Intravenous	Oral	Intravenous	Oral
Dose (mg/kg)	5	10	5	10
C_{max} (ng/mL)	NA	1180 ± 475	NA	426 ± 161
t_{max} (h)[a]	NA	4.00 (4.00)	NA	4.00 (2.00–4.00)
$t_{1/2}$ (h)	2.39 ± 0.172	NR	4.03 ± 0.966	3.79 ± 0.332
AUC_{0-t} (ng•h/mL)[b]	11,400 ± 815	14,200 ± 5520	4610 ± 630	2490 ± 1060
CL (mL/min/kg)	7.32 ± 5.43	NA	18.2 ± 2.73	NA
V_{ss} (L/kg)	1.19 ± 0.0262	NA	3.06 ± 0.361	NA
F (%)	NA	62.1 ± 24.1	NA	26.2 ± 8.3

Values are shown as the mean ± standard deviation of four animals

AUC_{0-t} area under the concentration–time curve from zero time to time of last quantifiable concentration, CL clearance, C_{max} maximum observed concentration, F absolute bioavailability, *NA* not applicable, *NR* not reportable, $t_{1/2}$ elimination phase half-life, t_{max} time to reach C_{max}, V_{ss} volume of distribution at steady state

[a]Median value (range)

[b]$t = 24$ h

in H3B-6545 CL_{int} was observed at 1.0 μM relative to 0.3 μM in rat, and monkey, while no concentration dependence was observed in human hepatocytes. These in vitro clearance rates over-predicted in vivo CL in nonclinical species, while applying a simple correction for free fraction in plasma had the opposite effect (Table 1). Both calculations suggested a need for free fraction correction (in vitro and in vivo), which was applied in the PBPK model. The control substrates diclofenac and metoprolol demonstrated the expected depletion in all species.

Metabolite identification of H3B-6545 in rat, monkey and human hepatocytes

The protonated molecular ion of H3B-6545 was m/z 568.23, and the accurate mass measurement provided the expected chemical formula of $C_{30}H_{30}F_4N_5O_2$. Figure 1 illustrates the proposed fragmentation pattern of H3B-6545. Structurally diagnostic ions were observed at m/z 440.14, 414.12, 155.12, 112.08, 110.06, 84.08 (112–CO) and 82.07. Metabolites showed similar diagnostic ions, which allowed for elucidation and proposal of their structures. A representative UPLC–MS chromatogram is presented in Fig. 2.

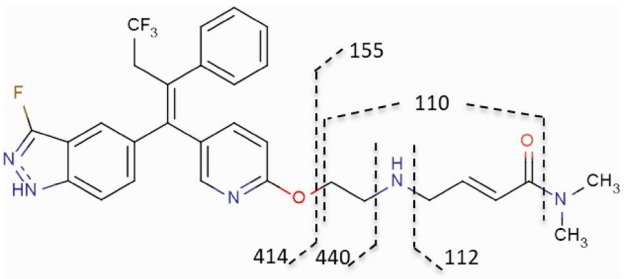

Fig. 1 H3B-6545 structure and proposed LC-MS fragmentation pattern. H3B-6545 diagnostic fragment ions generated with high resolution accurate mass were used to propose metabolite structures. In addition, m/z 82 (m/z 110-CO) was used as diagnostic ion

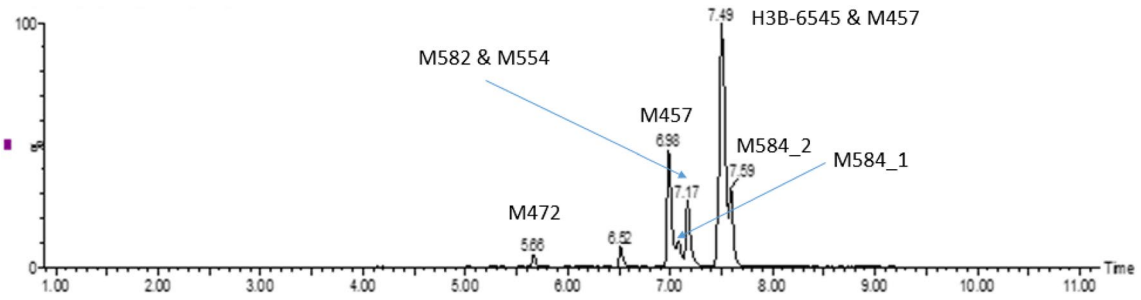

Fig. 2 Representative LC–MS/MS chromatogram: metabolite profile in pooled female human hepatocytes following 240 min of incubation with 10 µM H3B-6545. The peak at 6.52 min is an unknown impurity (present in negative control incubation)

Nine metabolites of H3B-6545 were identified in hepatocyte incubations, none of which were unique to humans (Fig. 3). In all species, based on total peak area mass spectrometry response (the sum of H3B-6545 and all metabolites), the prominent metabolic pathways for H3B-6545 were *N*-demethylation of the terminal amide (H3B-108945, m/z 554.22), *N*-dealkylation followed by oxidative deamination of the covalent side chain, generating M457 (m/z 457.16) and M458 (m/z 458.15), and oxidation of the side chain secondary amine (M584, m/z 584.23). A potential *N*-acetylglucosamine conjugation to H3B-6545 (M771, m/z 771.32) was detected in monkey and in trace amount in human hepatocytes only. The glutathione-conjugate of H3B-6545 (M875, m/z 875.32) represented less than 1% of the total MS peak area after 240 min of incubations. Other potential minor metabolites were detected (< 1% of total peak area).

Identification of human cytochrome P450 enzymes metabolizing H3B-6545 with prediction of contributions to hepatic CYP-mediated clearance

Depletion of the positive control carvediol was within historical range. No depletion of H3B-6545 (< 15%) was observed following incubations with recombinant CYP2E1. H3B-6545 was depleted in HLMs with a predicted CL_{int} of 553 µL/min/mg, corresponding to a scaled clearance of 20 mL/min/kg (97% Q_H), a value slightly higher than that obtained using human hepatocytes (Table 1). Using recombinant enzymes, H3B-6545 was predominantly metabolized by

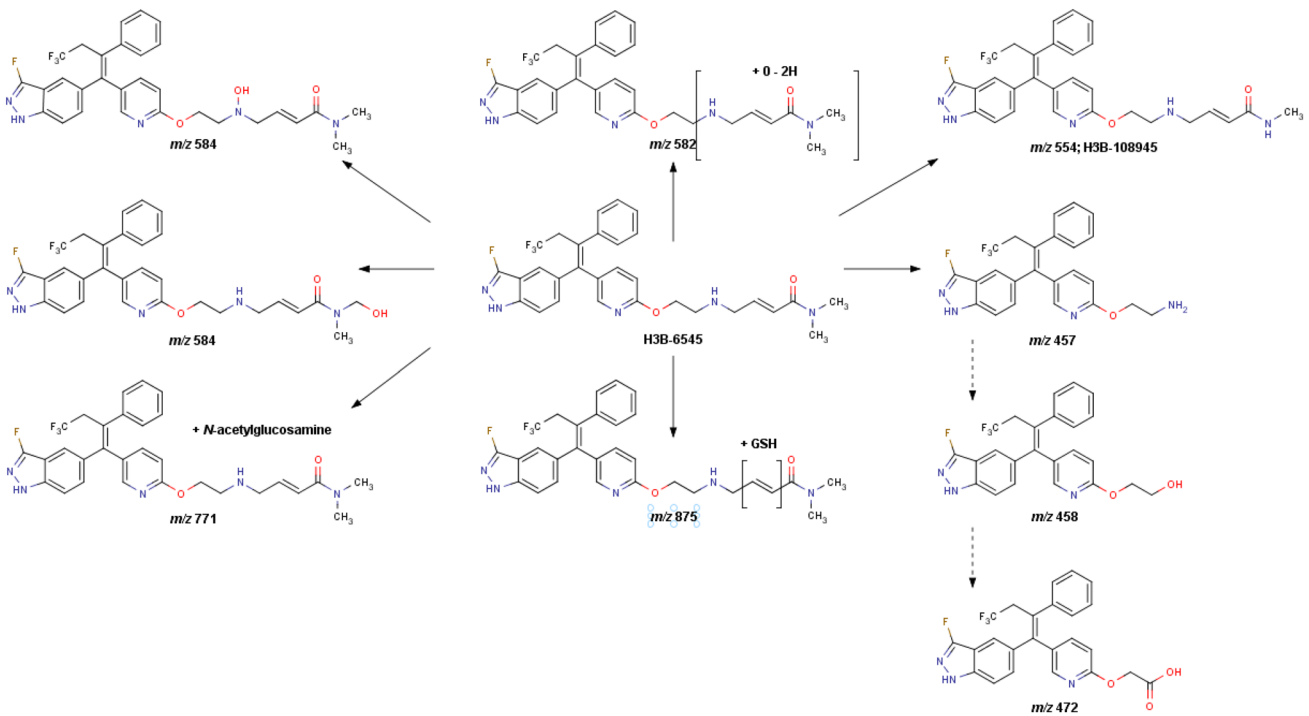

Fig. 3 Proposed major metabolic pathways of H3B-6545 in rat, monkey and human hepatocytes

CYP3A4 with a projected f_m of 84%, followed by CYP3A5 (8.9%), CYP2C8 (4.5%), and CYP2J2 (2.0%). CYP1A2, CYP2B6, CYP2C9, CYP2C19, and CYP2D6 minimally contributed to H3B-6545 clearance (f_m <1%).

In vitro evaluation of the substrate potential of H3B-6545 for P-glycoprotein and breast cancer resistance protein

At up to 20 µM, the P_{app} of lucifer yellow was less than 0.8×10^{-6} cm/s in all monolayers of all three cell lines, demonstrating that H3B-6545 did not compromise the MDCK monolayer integrity. The bidirectional permeability of digoxin and cladribine was as expected from the historical data, respectively, indicating a functional P-gp and BCRP test system. In MDCK cells, H3B-6545 showed moderate permeability with $P_{app(AP\text{-}to\text{-}BL)}$ values of 1.4, 2.9, and 2.4×10^{-6} cm/s at 0.3, 3, and 20 µM, respectively. In the P-gp substrate assessment, the net flux ratios (efflux ratio in MDR1-MDCK cells over that in MDCK cells) of H3B-6545 were 15.3, 18.0, and 10.4 at 0.3, 3, and 20 µM, respectively. Valspodar inhibited the efflux of H3B-6545 by 99.3%. In the BCRP substrate assessment, although the net flux ratios of H3B-6545 ranged from 3.1 to 4.3, Ko143 did not inhibit the efflux of H3B-6545. Therefore, H3B-6545 is a substrate of P-gp, but not a substrate of BCRP.

Determination of binding of H3B-6545 to rat, monkey and human plasma proteins

H3B-6545 showed similar high plasma protein binding across the nonclinical species and human (99.5–99.8%) and did not appear to have any concentration dependence from 1 to 10 µM (Table 1). In all cases, plasma stability following a 2.5-h incubation was ≥ 99.3%. Warfarin binding was as expected from historical data.

Determination of binding of H3B-6545 to human liver microsomes

Fraction unbound (f_u) of H3B-6545 (1 µM) decreased with increasing protein concentration. F_u values were 0.018, 0.010, and 0.007 at HLM concentrations of 0.5, 1.0 and 2.0 mg/mL, respectively. Verapamil binding was as expected from the historical data.

Pharmacokinetics

The plasma PK of H3B-6545 has been characterized in female Sprague–Dawley rats and cynomolgus monkeys, the species used in the nonclinical safety evaluation of H3B-6545 (Table 2). In both species, the concentration of H3B-6545 in pre-dose samples was below quantification limit (< 0.5 ng/mL). The PK disposition of H3B-6545 is characterized by a low CL in rats and a moderate CL in monkeys after IV administration, and the terminal elimination half-life ($t_{1/2}$) was 2.4 h in rats and 4.0 h in monkeys. Renal clearance was not a significant contributor to the elimination of H3B-6545 in rats, with less than 1% of the IV dose recovered as unchanged parent in urine. In both species, H3B-6545 appears to be widely distributed with a volume of distribution at steady state (V_{ss}) that exceeds total body water, at 1.2 L/kg in rats and 3.1 L/kg in monkeys. After oral dosing, absorption was prolonged with the time to the maximum plasma concentration (t_{max}) typically being achieved at 4 h. In a fasted state, the oral bioavailability (F) was low in monkeys (26.2%) and moderate in rats (62.1%).

Projection of human clearance and volume of distribution

A PBPK modeling approach was used to simulate H3B-6545 exposures in rat and monkey following a single IV administration and project human CL and V_{ss}.

Based on visual inspection, the model fit of H3B-6545 in rat and monkey adequately described the time-concentration profiles (Fig. 4) and resulted in prediction of mean CL, V_{ss} and AUC_{0-t} within ± 10% of the observed values in both species. This PBPK model projected a mean V_{ss} of 277 L (3.6 L/kg) and a CL of 5.6 mL/min/kg, translating to a mean projected half-life of 7.5 h for H3B-6545 in human.

Discussion

H3B-6545 is a novel Selective ERα Covalent Antagonist (SERCA), which inactivates both wild-type and mutant ERα, and recently initiated clinical development as an investigational new drug in metastatic breast cancer [8, ClinicalTrials.gov Identifier: NCT03250676]. In this study, we report on the absorption and metabolic fate and disposition of H3B-6545 in rats and monkeys, the species used for safety assessment. We also aim to illustrate that in vitro–in vivo correlation of clearance is possible for TCIs, provided reactivity is not a predominant mechanism of clearance.

Following a single IV dose administration, the PK distribution of H3B-6545 was characterized by a low CL in rats, and a moderate CL in monkeys. Very low renal CL was observed in rats suggestive of a passive glomerular filtration mechanism. In all species tested, H3B-6545 appears to be widely distributed with a V_{ss} that exceeds total body water [9]. After oral administration, H3B-6545 absorption was prolonged, and in line with the moderate permeability observed in MDCK cells. In addition, the resulting low to moderate bioavailability is consistent with the in vitro hepatocyte stability suggestive of first

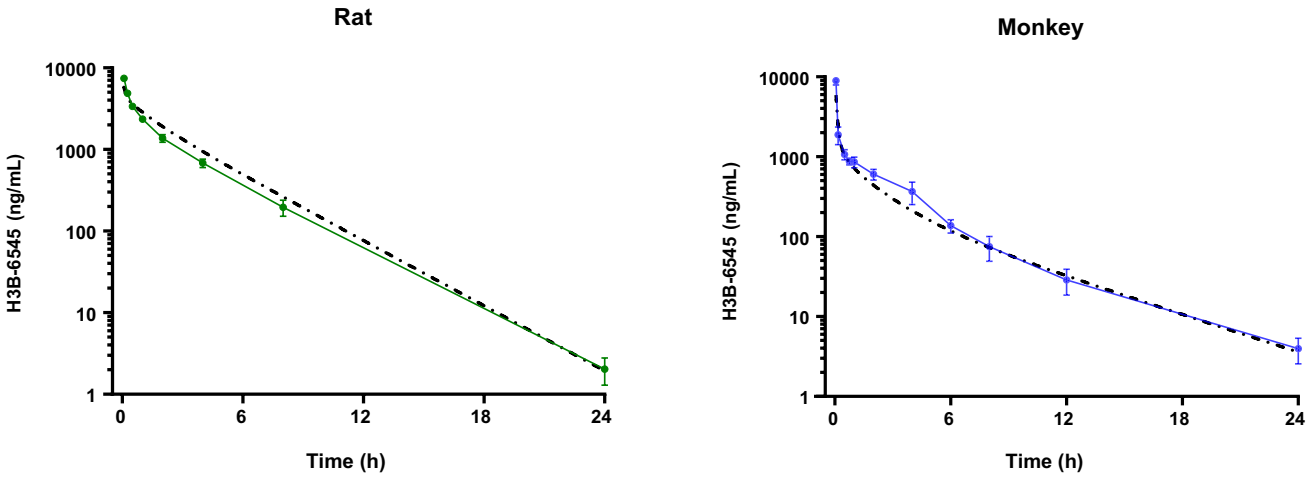

Fig. 4 Representative plot showing plasma exposure following a single IV administration at a dose of 5 mg/kg and the model fit for H3B-6545 in female **a** SD rat, and **b** cynomolgus monkey. Symbols represent observed data (mean of $n = 4 \pm$ SD) and the dashed line represents the mean profile projected in each nonclinical species from the PBPK model

pass metabolism. H3B-6545 binding to plasma proteins was extensive, yet relatively similar across species, at 99.5–99.8% bound, and no concentration-dependency was observed. H3B-6545 was also highly bound to human microsomal proteins. Applying the well-stirred model [14, 15], scaling of the hepatocyte data over-predicted in vivo CL (~ fivefold in nonclinical species), while correcting only for plasma protein binding would have under-predicted CL (≥ eightfold), a commonly reported finding for highly bound compounds [16].

Nine metabolites of H3B-6545 were identified in incubations of human hepatocytes, none of which were unique to humans, suggesting that rat and monkey are appropriate toxicology test species. In all species, the prominent metabolic pathways for H3B-6545 were demethylation, *N*-dealkylation, and oxidation of the sidechain. Noteworthy, the structure of the *N*-desmethyl metabolite of H3B-6545 was confirmed with a reference standard (H3B-108945). None of the proposed metabolites resulted from modifications to the H3B-6545 core. Other than a minimal amount of GSH conjugation, the only other primary phase 2 metabolite observed was a potential minor *N*-acetylglucosamine conjugate (M771), detected in monkey and human hepatocytes. Glycosylation of small lipophilic xenobiotics, via UDP glycosyltransferase (UGT), generates a metabolite more polar than the parent drug and thus is generally considered a detoxification pathway [17]. Using human recombinant CYP enzymes, the hepatic metabolism of H3B-6545 appears to be catalyzed predominantly by CYP3A4, CYP3A5, and to a lesser extent by CYP2C8. These results were consistent with reaction phenotyping studies conducted in HLM with chemical inhibitors which showed a $f_{m,CYP3A}$ of 0.92 (unpublished data).

Since H3B-6545 comprises a reactive acrylamide that can act as the electrophile in Michael addition, formation of covalent adducts to nucleophilic electron-rich molecules such as GSH and cysteine would not be unexpected. Conjugation with the cysteine moiety of GSH is a common route of TCI metabolism, both in vitro and in vivo [18–20]. GSH can either by added directly to the Michael acceptor and/or the reaction can be catalyzed by one or more hepatic or extrahepatic GSTs. Consequently, simple extrapolation from liver fractions or hepatocyte incubations may not be representative of in vivo CL, as shown for ibrutinib and neratinib [21]. Additionally, simple allometry may not predict human CL due to species differences in GST expression and activity [22]. To overcome this lack of correlation, recent studies suggest considering blood stability and cardiac output when projecting in vivo CL of TCIs [6]. This highlights the need to optimize screening cascades for TCIs to better understand routes of excretion. Another potential reason for IVIVC disconnect of TCIs is a potential for covalent binding to proteins, such as albumin, and relatively slow excretion in bound form, as reported for afatinib and osimertinib in clinical ADME studies [18, 23]. Mass balance studies of H3B-6545 in rats will be performed at a later time to refine our understanding of the compound excretion pathways. Since we demonstrated that H3B-6545 was stable in plasma, and observed low/moderate CL in vivo, associated with minimal GSH-related conjugation in hepatocytes, we proceeded with modeling of nonclinical PK to project human CL.

PBPK models can describe and/or predict PK parameters and simulate concentration–time curves profile of a given drug in plasma. Considerable experience has now accumulated with the development of PBPK models to describe drug concentration–time profiles in adults, and more recently

in cancer drug development [24]. The adequate plasma concentration–time profile fit obtained following modeling of the IV PK of H3B-6545 in both rat and monkey demonstrate that for TCIs such as H3B-6545, where hepatic metabolism is expected to be the predominant clearance pathway, a good prediction of in vivo clearance can be obtained using hepatocytes. With this relatively simple model, clearance in human was projected around 25% of hepatic blood flow. In conjunction with the V_{ss} value generated from the model, we projected the mean plasma half-life of H3B-6545 at approximately 7–8 h in a healthy adult female. This value guided the design of the phase I/II study dosing regimen.

Taken together, these findings provide an understanding of the metabolism of this new SERCA and were used to support species selection for safety evaluation. This study will also aid in our understanding of metabolic information generated in human studies.

Acknowledgements The authors want to thank the H3B-6545 team at H3 Biomedicine for fruitful discussions.

Funding This study was funded by H3 Biomedicine Inc.

Compliance with ethical standards

Conflict of interest The authors declare that they have no conflict of interest.

Research involving human and/or animal participants All applicable international, national, and/or institutional guidelines for the care and use of animals were followed.

References

1. Kauhava L, Immonen-Räihä P, Parvinen I, Holli K, Pylkkänen L, Kaljonen A, Helenius H, Kronqvist P, Klemi PJ (2008) Lower recurrence risk through mammographic screening reduces breast cancer treatment costs. Breast 17:550–554
2. Spicer DV, Pike MC (1993) Breast cancer prevention through modulation of endogenous hormones. Breast Cancer Res Treat 28:179–193
3. Beslija S, Bonneterre J, Burstein HJ et al (2009) Third consensus on medical treatment of metastatic breast cancer. Ann Oncol 20:1771–1785
4. Chandarlapaty S, Chen D, He W et al (2016) Prevalence of ESR1 mutations in cell-free DNA and outcomes in metastatic breast cancer: a secondary analysis of the BOLERO-2 clinical trial. JAMA Oncol 2:1310–1315
5. Puyang X, Furman C, Zheng GZ et al (2018) Discovery of selective estrogen receptor covalent antagonists for the treatment of ERα^{WT} and ERα^{MUT} breast cancer. Cancer Discov. https://doi.org/10.1158/2159-8290.CD-17-1229
6. Leung L, Yang X, Strelevitz TJ, Montgomery J, Brown MF, Zientek MA, Banfield C, Gilbert AM, Thorarensen A, Dowty ME (2017) Clearance prediction of targeted covalent inhibitors by in vitro–in vivo extrapolation of hepatic and extrahepatic clearance mechanisms. Drug Metab Dispos 45:1–7
7. Colombo F, Smith S, Korpal M, Hao MH, Nix D, O'Shea M, Prajapati S, Wang J, Warmuth M, Smith PG, Rioux N (2018) In vitro-in vito correlation of clearance for H3B-5942, a novel selective ERα covalent antagonist (SERCA). In: 22nd North American ISSX meeting, abstract P10. https://bib.irb.hr/datoteka/947954.22nd_north_american_issx_meeting_abstract_book.pdf
8. Smith PG, Puyang X, Furman C et al (2017) Discovery and development of H3B-6545: a novel, oral, selective estrogen receptor covalent antagonist (SERCA) for the treatment of breast cancer. In: Proceedings of the American Association for Cancer Research Annual Meeting 2017, AACR, Washington DC. Cancer Res 77(13 Suppl):Abstract nr DDT01-04
9. Davies B, Morris T (1993) Physiological parameters in laboratory animals and humans. Pharm Res 10:1093–1095
10. Pollack GM, Brouwer KLR, Demby KB, Jones JA (1990) Determination of hepatic blood flow in the rat using sequential infusions of indocyanine green and galactose. Drug Metab Dispos 18:197–202
11. Nakajima M, Nakamura S, Tokudome S, Shimada N, Yamazaki H, Yokoi T (1999) Azelastine *N*-demethylation by cytochrome P450 (CYP)3A4, CYP2D6, and CYP1A2 in human liver microsomes: evaluation of approach to predict the contribution of multiple CYPs. Drug Metab Dispos 27:1381–1391
12. Drug development and drug interactions: table of substrates, inhibitors and inducers. https://www.fda.gov/Drugs/DevelopmentApprovalProcess/DevelopmentResources/DrugInteractionsLabeling/ucm093664.htm Accessed 2 July 2018
13. Takenaka K, Morgan JA, Scheffer GL, Adachi M, Stewart CF, Sun D, Leggas M, Ejendal KF, Hrycyna CA, Schuetz JD (2007) Substrate overlap between Mrp4 and Abcg2/Bcrp affects purine analogue drug cytotoxicity and tissue distribution. Cancer Res 67:6965–6972
14. Gillette JR (1971) Factors affecting drug metabolism. Ann NY Acad Sci 179:43–66
15. Rowland M, Benet LZ, Graham GG (1973) Clearance concepts in pharmacokinetics. J Pharmacokinet Biopharm 1:123–136
16. Obach RS (1999) Prediction of human clearance of twenty-nine drugs from hepatic microsomal intrinsic clearance data: an examination of in vitro half-life approach and nonspecific binding to microsomes. Drug Metab Dispos 27:1350–1359
17. Mackenzie PI, Rogers A, Treloar J, Jorgensen BR, Miners JO, Meech R (2008) Identification of UDP glycosyltransferase 3A1 as a UDP *N*-acetylglucosaminyltransferase. J Biol Chem 283:36205–36210
18. Stopfer P, Marzin K, Narjes H, Gansser D, Shahidi M, Uttereuther-Fischer M, Ebner T (2012) Afatinib pharmacokinetics and metabolism after oral administration to healthy male volunteers. Cancer Chemother Pharmacol 69:1051–1061
19. Scheers E, Leclercq L, de Jong J, Bode N, Bockx M, Laenen A, Cuyckens F, Skee D, Murphy J, Sukbuntherng J, Mannens G (2015) Absorption, metabolism, and excretion of oral 14C radiolabeled ibrutinib: an open-label, phase I, single-dose study in healthy men. Drug Metab Dispos 43:289–297
20. Baillie TA (2016) Targeted covalent inhibitors for drug design. Angew Chem Int Ed 55:13408–13421
21. Shibata Y, Chiba M (2015) The role of extrahepatic metabolism in the pharmacokinetics of the targeted covalent inhibitors afatinib, ibrutinib, and neratinib. Drug Metab Dispos 43:375–384
22. Commandeur JN, Stijntjes GJ, Vermeulen NP (1995) Enzymes and transport systems involved in the formation and disposition of glutathione *S*-conjugates. Role of bioactivation and detoxification mechanisms of xenobiotics. Pharmacol Rev 47:271–330
23. Dickinson PA, Cantarini MV, Collier J, Frewer P, Martin S, Pickup K, Ballard P (2016) Metabolic disposition of osimertinib

in rats, dogs, and humans: insights into a drug designed to bind covalently to a cysteine residue of epidermal growth factor receptor. Drug Metab Dispos 44:1201–1212

24. Block M (2015) Physiologically based pharmacokinetic and pharmacodynamic modeling in cancer drug development: status, potential and gaps. Expert Opin Drug Metab Toxicol 11:743–756